Modeling of pressure loads during a premixed hydrogen combustion in the presence of water spray

G. Gai, S. Kudriakov, A. Hadjadj, E. Studer, Olivier Thomine

HAL Id: cea-02339715
https://cea.hal.science/cea-02339715

Modeling of pressure loads during a premixed hydrogen combustion in the presence of water spray

Guodong Gai[a,*], Sergey Kudriakov[a], Abdellah Hadjadj[b], Etienne Studer[a], Olivier Thomine[a]

[a]*DEN-DM2S-STMF, CEA, Université Paris-Saclay, France*
[b]*Normandie University, INSA of Rouen, CNRS, CORIA, 76000 Rouen, France*

Abstract

This paper describes the development of a simplified model for pressure evolution inside a closed volume during a combustion process in presence of a water spray. The model is based on empirical correlations available in the literature. These ingredients allow us to estimate the values for the main factors influencing the pressure evolution. The results of this model are used as a guideline for adjusting the parameters of a three-dimensional hydrodynamic code based on CREBCOM combustion model, developed and validated for large-scale hydrogen combustion. The methodology is successfully assessed by comparing the computed results with the experimental data of Carlson et al. [1].

Keywords:
Combustion, Water spray, CFD, Hydrogen Safety, PWR

1. Introduction

During certain severe accident scenarios in a nuclear Pressurized Water Reactor (PWR) containment building, gaseous hydrogen, produced by a reactor core oxidation, can be released from the reactor coolant system and mix with the air-steam flux. In the case of ignition, various combustion regimes are possible depending on the local concentrations of hydrogen and steam, as well as pressure and temperature distributions.

---

*Corresponding author
   Email address:* `guodong.gai@cea.fr` (Guodong Gai)

Nomenclature

$a_{0.5}$	Averaged heat flux, W/cm^2
c_{sp}	sound speed in the combustion products, m/s
c_v	constant volume specific heat, $J/kg/K$
D	diameter of the droplet, m
e	specific energy, J/kg
h	specific enthalpy, J/kg
H	volumetric heat transfer coefficient, $W/m^3/K$
I	static pressure impulse, $bar.s$
K_0	parameter related to flame velocity in CREBCOM model, m/s
l	latent heat of evaporation, kJ/kg
L	length of the experimental tube, m
Le	Lewis number, dimensionless
L_T	integral length scale, m
N	ratio of the flame surface to the tube cross-section area, dimensionless
p_{max}	maximum pressure, bar
Q	heat transfer coefficient, $kW/m^2/K$
Q_w	supply flow rate, l/s
$\mathcal{R}$	universal gas constant, $J/K/mol$
S_L	laminar flame velocity, m/s
S_t	turbulent flame velocity, m/s
t_{max}	time needed for the flame to reach the maximum pressure, s
W	molar mass, kg/mol
x_{H_2}	molar fraction of hydrogen
α	liquid volumetric fraction, dimensionless
$\dot{\alpha}$	volumetric evaporation rate, s^{-1}
γ	specific heat ratio
δ	flame thickness, m
Δx	average cell size, cm
ρ	mass density, kg/m^3
σ	Expansion ratio between density of unburnt and burnt gases, dimensionless
Σ	flame surface, m^2
Ψ	criterion function for the ignition, dimensionless
ω	chemical reaction rate, s^{-1}

The spray systems are emergency devices designed for preserving the containment integrity in case of a severe accident in a PWR. These spray systems are used to limit the overpressure, enhance the gas mixing, avoid hydrogen accumulation, and wash out the fission products and the structure materials that may be released into the reactor building [2]. Depending on the accident scenario evolution, ignition might occur *after* the activation of the spray system. Thus an understanding of i) the dynamics of water spray exposed to explosion-induced flow field, and ii) the spray ability to mitigate the explosion are needed.

In order to improve hydrogen risk management strategies, one has to find means to estimate the severity of combustion process involved into various regimes of flame propagation, including turbulent deflagration-spray interaction phenomenon.

A wealth of research material on flame-spray interaction phenomenon related to explosion mitigation in industrial environments is available in the open literature. In [3], [4] a rather thorough analysis of main factors influencing flame evolution during spraying is presented. Early small scale experiments [5] as well as recent small and medium scale experiments using hydrogen [6], [7], [8], [9] have revealed that sprays containing small-size droplets, of the order of $\mathcal{O}(10 \ \mu m)$ can be effective against premixed combustion.

Droplets generated by industrial water-spray systems are relatively large, having diameters of the order of $\mathcal{O}(100-1000 \ \mu m)$, and these droplets will hardly evaporate in a flame propagating through a premixed gas mixture. Nevertheless, several studies [10] have indicated that water sprays can lead to a significant reduction in explosion overpressure. The primary mechanism that leads to mitigation is believed to be a reduction in mean droplet size as a result of aerodynamic interactions between the droplet and the explosion-induced flow field. The mitigation action of the spraysis then attributed to the interaction of this finer spray with the combustion wave. Another results [10], [11] have shown that there are certain circumstances under which the presence of spray can cause a propagating flame to accelerate, as a result of the turbulence induced by spray, leading to a higher overpressure.

The pressure evolution brought by turbulent combustion, as can be seen from the above paragraph, in the presence of spray is a result of interplay of several factors, such as i) turbulent combustion rate, ii) convective heat loss rate to internal solid structures and to water droplets, iii) heat loss rate due to droplet evaporation. A physical model should be able not only to incorporate these effects and reproduce a pressure signal, but also to do so at a large geometrical scale, typical of a reactor building.

The difficulties related to this task are twofold: i) combustion models integrated into the current *large-scale* numerical codes experience poor predictive capabilities

3

[12], and ii) the experimental data devoted to turbulent combustion-spray interaction, due to inherent difficulties, often contain only pressure evolution and flame trajectory along some direction [1], [13]. These data are not sufficient for code validation as they do not allow a correct estimation of order of magnitude for each of the above-mentioned factors.

In this paper, we describe the development of a simplified numerical model of pressure evolution inside a closed volume during a combustion process in presence of a water spray. The model is based on empirical correlations found in the open literature. These ingredients allow us to estimate the values for the main factors influencing the pressure evolution. The results of this model are used as a guideline for adjusting the parameters of a three-dimensional hydrodynamic code based on CREBCOM combustion model, developed and validated for large-scale hydrogen combustion [14], [15], [16]. The main idea is to keep the CFD code as simple as possible by using explicitly the available experimental data, thus gaining in efficiency and predictability.

2. Methodology

The following approach is adapted in order to determine the pressure loads during turbulent combustion in the presence of spray:

- Based on a simplified numerical model for pressure evolution inside a closed volume, developed under low-Mach number hypothesis, we reveal the main mechanisms and lumped-parameter factors, such as turbulence combustion rate, volumetric heat-loss coefficient and volumetric water-evaporation rate, leading to a given pressure evolution.

- Using available experimental data and empirical correlations, we estimate the values of the main factors defined above and perform a sensitivity study based on Design of Experiments (DOE) approach.

- The outcomes of the two previous steps will serve as a guideline for adjusting the parameters of a full three-dimensional hydrodynamic code based on CREBCOM combustion model.

The present methodology will be demonstrated using a medium-scale experimental data of [1], briefly described here.
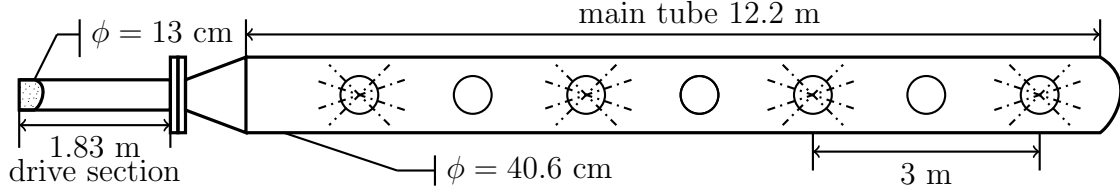
Figure 1: Sketch of the facility showing the location of spray nozzles used in [1].
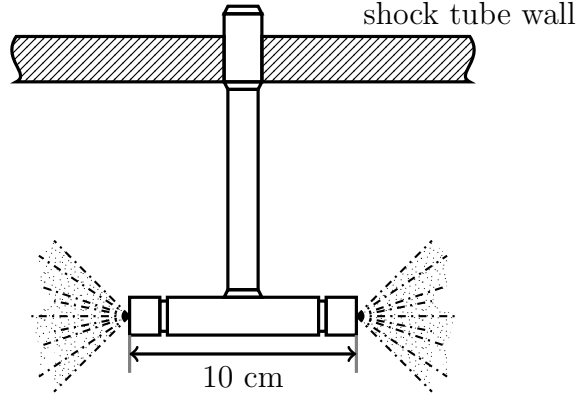

Figure 2: Water spray nozzle detail reproduced from [1].

2.1. Experiments of Carlson et al. [1]

In this experiments, a shock tube was used as a main device. It consists of a long section carbon steel pipe of length $L_{tube} = 12.2$ m and diameter $D_{tube} = 40.6$ cm, which is welded closed on one end. The other end of the tube is connected to a small-diameter driver tube ($L_{driver} = 1.83$ m, $D_{driver} = 13$ cm) through two standard bell reducers, as shown in Fig.1.

A sketch of the nozzle setup is shown in Fig. 1. Sufficient spray density was realized from the four sets of nozzles, as schematically depicted by dashed lines. The two nozzles spray in opposite directions along the shock tube as shown in Fig. 2. The test program kept the same spraying system as used in commercial reactor at comparable spacings and operating at equivalent pressure level ($\triangle p \approx 4.1$ bar). The authors indicate that the mean droplet diameter is $D_p \approx 500$ μm. They estimated that the liquid volumetric fraction is $\alpha = 5 \times 10^{-4}$, which is comparable to the containment spray system liquid volume fraction in a nuclear plant.

A total of 22 tests were conducted, with hydrogen concentration ranging from 5%

Table 1: Operating conditions for the flame test cases.

Test No.	x_{H_2} (dry)	Q (l/s)	p_0 (bar)	p_{max} (bar)
7	16.0	0.0	1.013	3.36
8	16.0	4.6	1.013	1.97

to 16% (dry air concentrations) and initial pressure from 1 bar to 2 bar. Here, we consider two tests, and the corresponding initial conditions together with maximum pressure values measured during these experiments are presented in Table 1. The experimental results show that the water spray reduces the maximum pressure in the shock tube, as well as the time for the pressure elevation with regards to its initial value. The heat losses play an important role during the combustion process (see Fig. 3), as the maximum pressure is much lower than the adiabatic isochoric complete combustion (AICC) pressure. Note that in both tests, 7 and 8, $p_{AICC} = 5.9$ bar.
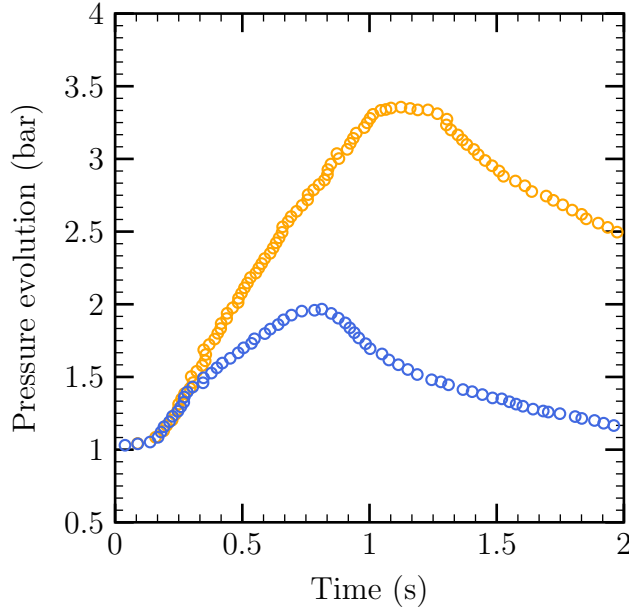

Figure 3: Pressure evolution as a function of time, results of Test 7 (o) and Test 8 (o). Scanned from [1]

2.2. Simplified numerical model analysis

Here, we present a reduced-order model for pressure evolution inside a closed tube, developed under low-Mach number assumption. The purpose is twofold: i) reveal the main mechanisms leading to a particular pressure evolution; ii) build a framework for sensitivity analysis that will be outlined later.
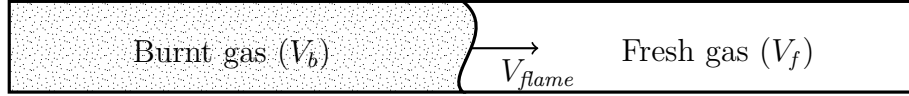

Figure 4: Schematic representation of a flame propagation along a tube.

The model is based on sensible enthalpy conservation law [17]. Taking into account the fact that combustion takes place at low-Mach number regime, by integration we can have the ordinary differential equation for the pressure evolution inside the tube (see Appendix A for derivation details):

$$\frac{d}{dt}\left[p\left(\frac{\gamma_b}{\gamma_b - 1}V_b + \frac{\gamma_f}{\gamma_f - 1}V_f - V_{tot}\right)\right] = \Sigma \cdot S_L \cdot \triangle H \cdot \rho_f \cdot Y_{H_2}$$
$$-H\left(\frac{p}{\rho_b R_b}V_b + \frac{p}{\rho_f R_f}V_f - T_0 V_{tot}\right) \tag{1}$$

where p is the thermodynamic pressure, $V_b(t)$ and $V_f(t)$ are the volumes occupied by burnt and fresh gases, respectively (see Fig. 4). The closed volume is represented by V_{tot}, H is the *volumetric* heat loss coefficient, T_0 is the reference temperature, Σ is the flame surface, S_L is the laminar flame velocity, ΔH is the energy release per kg of burnt hydrogen gas, ρ_f is the fresh gas density, and Y_{H2} is the mass fraction of hydrogen gas in the fresh mixture.

In case of spraying, another term has to be included in the right-hand side of Eq. (1). This term represents the energy losses related to the water evaporation, which can be expressed as:

$$-\rho_l \cdot \dot{\alpha} \cdot l \cdot V_b, \tag{2}$$

where ρ_l is the liquid density, l is the latent heat of evaporation, and $\dot{\alpha}$ is the liquid volume fraction rate of evaporation. For simplicity, we assume that the evaporation takes place only inside the burnt volume.

Several variables in Eq. (1) have to be modeled: i) the volume of the burnt gas evolution (V_b), ii) the flame surface evolution (Σ), and iii) the evolution of the volumetric heat loss coefficient.

Evolution of the volume of the burnt gas is closely related to the visible flame velocity evolution. The latter can be expressed as a sum of the gas velocity on the flame upstream side v_{gas} and the averaged burning velocity S_t, i.e.

$$v_{flame} = v_{gas} + S_t \tag{3}$$

For the burning velocity, S_t, the following expression is used:

$$S_t = S_L \frac{\Sigma}{A_{tube}} = S_L \cdot N, \tag{4}$$

where A_{tube} is the cross sectional area of the combustion tube. We make sure that the burning velocity stays lower than the visible flame velocity. As a first approach, we shall adapt constant values for H and N.

The solution algorithm is given in Appendix B.

2.2.1. Model application for Test 8 (with spray)

Here we shall apply the above model for Test 8. The spray was activated before the combustion, and the mixture properties are given in Table 2.

x_{H2}	S_L (m/s)	γ_f	γ_b	R_f (J/kg/K)	R_b (J/kg/K)
0.16	0.445	1.40	1.29	338.6	311.5

Table 2: Thermodynamic properties related to initial (subscript f) and final (subscript b) mixture properties.

As an example, we first fix the averaged flame velocity at a given value, $v_{flame}^{av} = 13$ m/s ($L_{tube} = 12.2$ m, the combustion takes less than 1 s), and consider three cases with different parameters for energy loss coefficient and the volumetric evaporation rate (see Table 3). The purpose of this exercise is to show that *very similar* pressure evolutions can be obtained using *different* sets of model parameters. The values for the parameters might not be physical; their correct estimation is the subject of the next subsections.

The pressure evolutions computed using the proposed model display relatively similar character (see Fig. 5). Moreover, the maximum pressure values are almost the same and take place at close time instants: $p^{max} = 1.96$ bar at $t = 0.816$ s (for Case 1), $p^{max} = 1.953$ bar at $t = 0.802$ s (for Case 2) and $p^{max} = 1.986$ bar at $t = 0.814$ s (for Case 3). We compute the pressure evolution over time, known as the pressure impulse, as:

$$I_p(t) = \int_0^t p(t') \, dt', \tag{5}$$

8

Case	H_1 (kW/K/m³)	H_2 (kW/K/m³)	v_{flame}^{av} (m/s)	$\dot{\alpha}$ (s^{-1})	N (-)
1	6	3	13	2.2×10^{-4}	30
2	5	3	13	4.4×10^{-4}	30
3	3	3	13	8.7×10^{-4}	30

Table 3: *Test 8*. Values used in the model. H_1 is the energy loss coefficient during combustion, H_2 is the energy loss coefficient after combustion.

The computed pressure impulse closely follows the experimental impulse evolution curve shown in Fig. 6. Note that the values of both maximum pressure p_{max} and impulse I_p are used for damage evaluation using P-I diagrams [18].
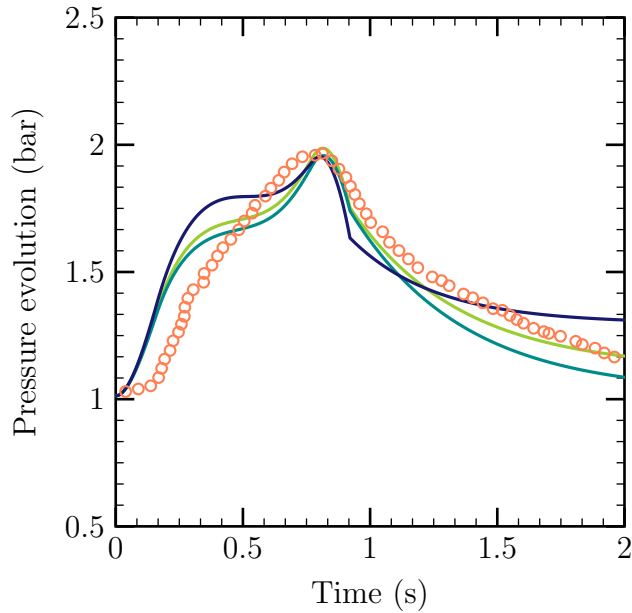

Figure 5: *Test 8*. Experimental pressure evolution (○) compared with computed pressure evolutions using $H_1 = 6000W/K/m^3$, $\dot{\alpha} = 2.2 \times 10^{-4} s^{-1}$ (——); $H_1 = 3000W/K/m^3$, $\dot{\alpha} = 8.7 \times 10^{-4} s^{-1}$ (——); and $H_1 = 5000W/K/m^3$, $\dot{\alpha} = 4.4 \times 10^{-4} s^{-1}$ (——).

We can observe that similar pressure evolution behavior can be obtained using different combinations of model parameters. We need more refined estimations or experimental data for both parameters, H and $\dot{\alpha}$.
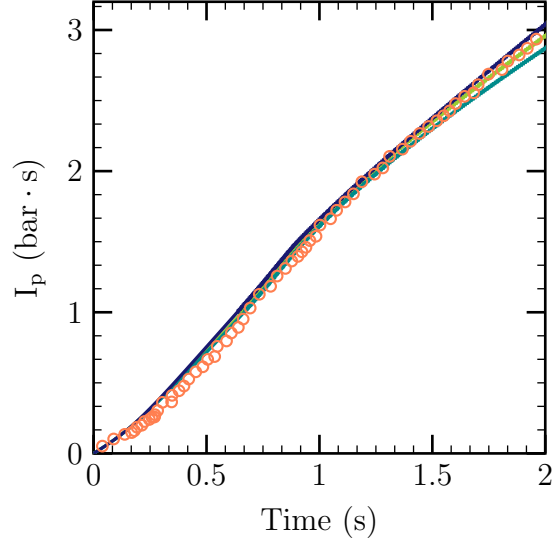
Figure 6: *Test 8.* Comparison between impulse evolutions corresponding to the experimental data (○) and to the computed data $H_1 = 6000W/K/m^3$, $\dot{\alpha} = 2.2 \times 10^{-4}s^{-1}$ (——); $H_1 = 3000W/K/m^3$, $\dot{\alpha} = 8.7 \times 10^{-4}s^{-1}$ (——); and $H_1 = 5000W/K/m^3$, $\dot{\alpha} = 4.4 \times 10^{-4}s^{-1}$ (——).

2.3. Estimation of the parameters

From the above subsection, we note that there are several main mechanisms which can lead to a particular pressure evolution:

- Combustion rate evolution

- Convective heat loss rate to the structure and droplets

- Heat loss rate due to droplet evaporation

Hence, in order to correctly model the thermodynamic system in terms of pressure evolution, one needs to have an estimation (an order of magnitude) of different parameters related to these mechanisms. In the present section, we shall attempt to estimate some of these parameters using the experimental correlations.

2.3.1. Estimation of the averaged evaporation rate $\dot{\alpha}$

The results of [19] are used in order to estimate the mass evaporation rate of a single droplet subjected to a gas flow around it. An approximate model of moving droplet evaporation has been formulated. The *two-films* model has been adopted to describe both the gas and the liquid phases, which is described by an *effective conductivity model*.
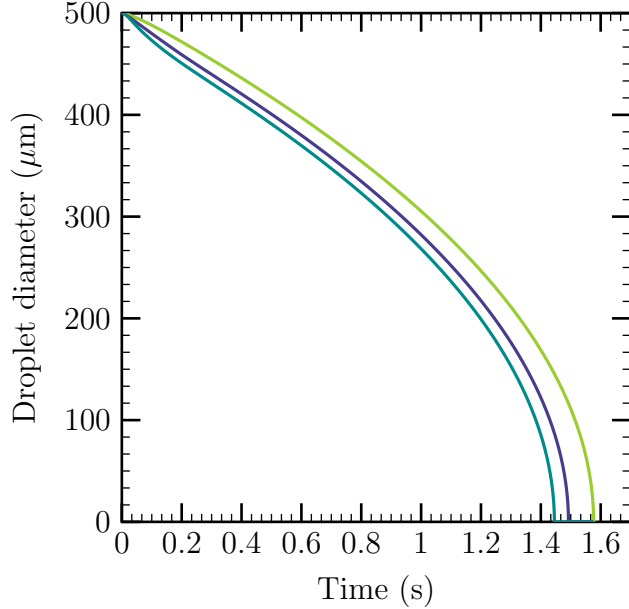
Figure 7: Diameter evolution of a single droplet, comparison between three models: conductivity limiting model (———), effective conductivity model (———) and conductivity infinity model (———).

By applying the theory developed in [19], one can compute the diameter evolution of a single droplet under high temperature, $T_{gas}^{AIBC} \approx 1547$ K. This temperature corresponds to adiabatic isobaric complete combustion (AIBC). A comparison between the *effective conductivity model* and the other two models applied to a droplet of $D_{droplet} = 500$ μm (corresponding to the droplet diameter of experiments [1]) and $T_{ini} = 373$ K, is given in the Fig. 7, from which we can see the variation of evaporation time in three different cases. The time taken for total evaporation varies for different models: infinite conductivity model (1.44 s), effective conductivity model (1.49 s) and conduction limit model (1.58 s). However, the estimated values are very close to each other.

Fig. 8 shows the variation of evaporation rate evolution for different ambient temperatures. Note that the temperatures corresponding to AIBC (1547 K) and AICC (1885 K) combustion are taken into consideration, as well as two temperatures (900 K and 1200 K) for comparison. We can see that the evaporation rate strongly depends on the ambient temperature of the gas phase. One can also estimate that the mean evaporation rate of one sigle droplet during the combustion process is of magnitude of $\mathcal{O}(10^{-8})$ kg/s.
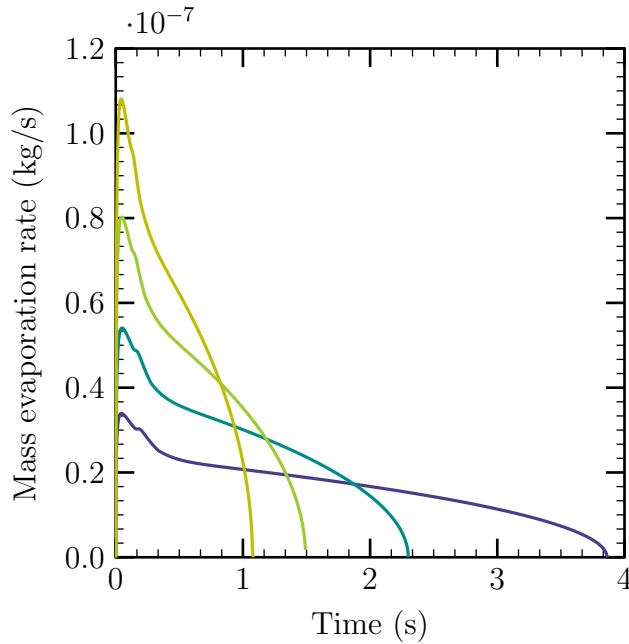
Figure 8: Influence of ambiant temperature on the mass evaporation rate: 900 K (——), 1200 K (——), $T^{AIBC} = 1547$ K (——) and $T^{AICC} = 1885$ K (——).

The volumetric spray evaporation rate can be estimated by the distribution of the water droplets in the computational space. In the experiment of [1], the number of droplets per unit volume for a single spray and the two opposing sprays in the shock tube are given in Fig. 9.

By integrating this curve in space, we can have the mean density of droplets between two nozzles:

$$N_{droplets} = 1.367 \times 10^6 \ m^{-3} \tag{6}$$

as well as the volume fraction of the spray between two successive nozzles:

$$\alpha = \frac{V_{liq}}{V_{tot}} = 8.9 \times 10^{-5} \tag{7}$$

We note that this value for liquid volume fraction is different from the one given by the authors (5.0×10^{-4}) [1]. In order to simplify the computation, we propose the following assumptions:

- All droplets are suspended in the shock tube and will take part in the evaporation process;
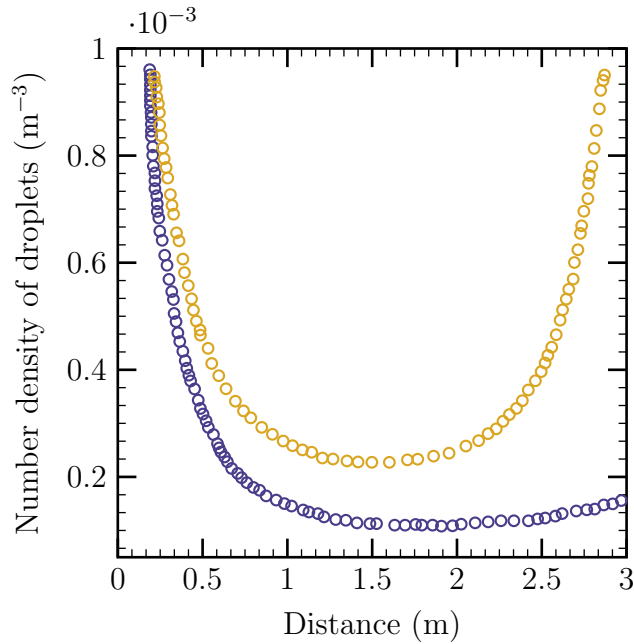
12

Figure 9: Droplet population density as a function of axial position between spray nozzles in the shock tube; single spray ○, two sprays ○ [1]

- The mass flow rate of the nozzle is constant during the combustion process;

- All droplets have the same mean diameter, which is fixed at $D_p = 500\ \mu$m;

- The number density of spray in terms of number of droplets per unit volume is kept constant.

By assuming that all droplets have the same mean diameter, we implicitly imply that the droplet break-up doesnot take place. The average flame velocity can be estimated by using the time instant when the pressure reaches its maximum value, i.e. the average flame velocity $v_{flame}^{av} \approx 13\ m/s$, which would give the Weber number:

$$W_e = \frac{\rho v^2 D_p}{\sigma} = 1.2 \tag{8}$$

where ρ is the density of the droplet, v is its velocity, D_p is the diameter of the droplet and σ is the surface tension. One notes that this value is an order of magnitude smaller than the critical Weber number $W_e = 12$.

13

From these assumptions, the mean volume evaporation rate can be calculated to describe the mean evaporation rate of the liquid phase:

$$\dot{\alpha} = \frac{\dot{m}_0 \times N_{droplets}}{\rho_l} \tag{9}$$

where $\dot{m}_0$ is the averaged mass evaporation rate of a single droplet, $N_{droplets}$ the density of the spray in terms of number of droplets per unit volume, ρ_l the density of water droplets. After calculation, we can obtain the volume evaporation rate:

$$\dot{\alpha} = 6.01 \times 10^{-5} \ s^{-1} \tag{10}$$

2.3.2. Volumetric heat loss coefficient H [20]

It is shown in [20] that the main mechanism for heat loss from the combustion products of propagating turbulent flames in obstructed tubes is the convective heat transfer. The function of the estimated heat exchange coefficient on the flame speed is presented in Fig. 10. It is obtained by mounting the thermal gauges to the inner surface of the tube to measure the overall heat flux.

The heat transfer coefficient is defined as:

$$Q = \frac{a_{0.5}}{T_c - T_0} \tag{11}$$

where T_c is the adiabatic isochoric combustion temperature of the mixture, T_0 is the ambient temperature, and $a_{0.5}$ is the averaged heat flux. Thus, the volumetric heat loss coefficient can be calculated by:

$$H = Q \frac{S_{tot}}{V_{tot}} \tag{12}$$

where S_{tot} is the total surface of the tube, V_{tot} the volume of the system. For instance, a fraction of 16% hydrogen-air mixture will give a mean flame velocity close to 20 m/s in the tube, thus we can deduce the value for H:

$$Q = 0.14 \ kW/m^2/K \rightarrow H = 4350 \ W/m^3/K \tag{13}$$

This estimation, as emphasized in [20], has a relative error of 50%.

2.3.3. Sensitivity analysis with respect to the flow parameters

Effects of the different flow parameters and their uncertainty on the pressure evolution can be quantified to complete the assessment of the developed model. In our case, the Design-of-Experiments techniques [21] have been applied to optimise the number of calculations and perform the sensitivity analysis.
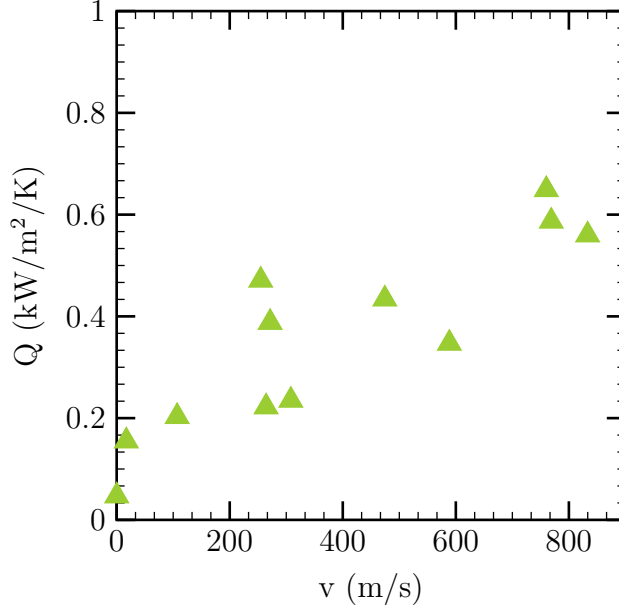
14

Figure 10: Heat transfer coefficient as a function of visible turbulent flame velocity [20].

Four factors (namely the volume fraction evaporation rate $\dot{\alpha}$, the volumetric heat transfer coefficient H, the ratio of the flame surface to tube cross-section area N, the laminar flame velocity S_L) have been chosen to investigate their effects on the responses variables (p_{max} maximum pressure, t_{max} time to reach the maximum pressure, I_p pressure impulse of pressure during the combustion computed up to 2 s). The variations chosen for all these parameters are summarized in Table 4. These variations come from estimated experimental uncertainty or engineering approximations.

Table 4: Selected parameters for the sensitivity study

Parameter	Unit	Min	Mean	Max
$\dot{\alpha}$	s^{-1}	3.0×10^{-5}	6.0×10^{-5}	9.0×10^{-5}
H	$Wm^{-3}K^{-1}$	2200	4350	6500
N	-	20	30	40
S_L	m/s	0.32	0.45	0.58

A 2_{IV}^{4-1} fractional factorial design has been selected taking into account the main

effects of single parameter and their 2-order interactions. Denote -1 the minimal estimated value for one parameter, and +1 the maximal value for this factor. The fractional factorial design can be expressed in Table 5 [22]:

Table 5: DOE Matrix for main factor and 2-order interactions

	$\dot{\alpha}$	H	N	S_L	$\dot{\alpha}H$	$\dot{\alpha}N$	HN
1	-1	-1	-1	-1	+1	+1	+1
2	-1	-1	+1	+1	+1	-1	-1
3	-1	+1	-1	+1	-1	+1	-1
4	-1	+1	+1	-1	-1	-1	+1
5	+1	-1	-1	+1	-1	-1	+1
6	+1	-1	+1	-1	-1	+1	-1
7	+1	+1	-1	-1	+1	-1	-1
8	+1	+1	+1	+1	+1	+1	+1

One can describe the reponses by a quadratic model:

$$\mathcal{Y} = \mathcal{Y}_0 \left(1 + \sum_{i=1}^{4} \mathcal{E}_i x_i + \sum_{j=1}^{2} \sum_{k>j}^{3} \mathcal{E}_{jk}\, x_j\, x_k \right) \tag{14}$$

where $\mathcal{Y}$ is the response, $\mathcal{Y}_0$ is the mean value for the response, x the studied parameter ($x = +1$ for maximal value, -1 for minimal value), $\mathcal{E}_i$, $\mathcal{E}_{jk}$ are the main effect coefficient of parameter x_i and interaction effect of two parameters x_j and x_k, respectively.

The determination of these coefficients requires 8 calculations using the matrix shown in Table 5, where each column corresponds to a parameter and each row represents a calculation. For example, the main effect coefficient of the volume evaporation rate can be calculated by:

$$\mathcal{E}_{\dot{\alpha}} = \frac{1}{2\mathcal{Y}_0} \left(\frac{y_5 + y_6 + y_7 + y_8}{4} - \frac{y_1 + y_2 + y_3 + y_4}{4} \right) \tag{15}$$

where y_i are the responses of the i-th calculation, the factor $\frac{1}{2}$ comes from the superposition of the main effect $\dot{\alpha}$ and a higher order interaction of other parameters.

The sensitivity analysis has been applied for the proposed model and the results are listed in Table 6, where the coefficients are expressed in terms of fraction of response $\mathcal{Y}$ mean values. For example, setting the heat transfer coefficient H to its

16

Table 6: Results of the sensitivity analysis: influence of the parameters on the responses

	t_{max} (s,%)	p_{max} (bar,%)	I (bar·s,%)
$\mathcal{Y}_0$	0.812	2.62	3.57
$\mathcal{E}_{\dot{\alpha}}$	-0.98	-0.22	-0.45
$\mathcal{E}_H$	-2.91	**-23.67**	**-19.07**
$\mathcal{E}_N$	**-9.07**	0.94	2.41
$\mathcal{E}_{S_L}$	-4.62	0.45	0.82
$\mathcal{E}_{\dot{\alpha}\cdot H}$	-2.58	1.40	-0.98
$\mathcal{E}_{\dot{\alpha}\cdot N}$	-1.21	-0.47	-1.39
$\mathcal{E}_{H\cdot N}$	-1.85	-1.02	-2.34

maximal value (+1 in Table 5, $H = 6500 \ W/m^3/K$) leads to a decrease (-sign in Table 6) of p_{max} by 23.67% from its mean value.

It can be deduced from Table 6 that the flame velocity, which is translated in time to reach the maximum pressure, t_{max} depends mainly on the flame surface, which is related to the turbulence level. The variation of the ratio between the flame surface and the cross-section area by 33% can change t_{max} by 9.07%.

The maximal pressure p_{max} is mainly affected by the heat transfer coefficient H as well as the flame surface area N. If one increases the volumetric evaporation rate $\dot{\alpha}$ or the heat transfer coefficient H, the maximal pressure will be reduced, since the evaporation and the heat transfer can take out energy from the system. However, if the flame surface is increased, the peak pressure will be elevated. The faster the flame propagates the higher the maximal pressure p_{max} and its impulse I will be.

The heat transfer coefficient has a most important influence on the impulse I. This is firstly due to the experiment uncertainty of H. According to [20], the uncertainty of estimated H is 50%. It seems that the evaporation of the water droplets has less important influence than the variation of the heat transfer on the pressure evolution, in spite of the same degree of uncertainty.

Finally, we can see that the interaction between the parameters have less importance than the contributions of the main factors.

3. CFD simulation with CREBCOM model

In this section, the medium-scale experiments of Carlson et al. [1] have been investigated by the CREBCOM combustion model [14], to analyze the overpressure and the flame velocity. A vaporization model has been used to reproduce some of the experimental data.
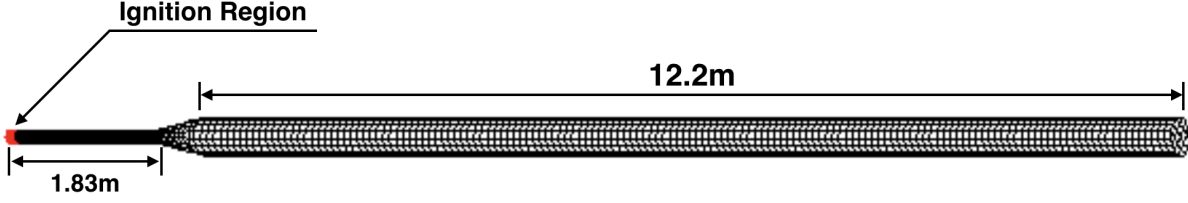
Figure 11: Geometry of a tube of two sections: 1.83 m (D_{driver} = 0.13 m) and 12.2 m (D_{tube} = 0.406 m); red color stands for the ignition region

In order to fit with the experimental setup, we define a tube composed of three parts: the 1.83 m drive cylinder of diameter 0.13 m, the 12.2 m main tube with spray system of diameter 0.406 m and the middle section which relates the two cylinders of different sections, as described in Fig. 11.

In our model, a thin layer of cells at the left end of the driven tube is chosen to be the ignition region (Fig. 11). For the thermodynamic conditions assigned to the ignition zone, we chose the final state of the same initial composition corresponding to the AICC conditions. For the first computations, we use a mesh of approximate cell size of $\Delta x = 10$ cm in the main tube. We have chosen a series of equidistant transducers located in the main tube for tracking the flame arrival time.

3.1. Governing equations

The system of equations solved are: 1) the reactive Euler equations for a mixture of H_2, O_2, H_2O and N_2, which express the conservation of total mass, the mass conservation for species k ($k = H_2, O_2, H_2O$), conservation of momentum and energy, and 2) the transport equations for $K_0, Y_{H_2,i}$ and $Y_{H_2,f}$ the meaning of which will be explained below.

$$\frac{\partial \rho}{\partial t} + \vec{\nabla} \cdot (\rho \vec{u}) = 0 \tag{16}$$

$$\frac{\partial \rho Y_k}{\partial t} + \vec{\nabla} \cdot (\rho \vec{u} Y_k) = \rho \dot{\omega}_k \tag{17}$$

$$\frac{\partial \rho \vec{u}}{\partial t} + \vec{\nabla} \cdot (\rho \vec{u} \otimes \vec{u} + p\boldsymbol{I}) = \rho \vec{g} \tag{18}$$

$$\frac{\partial \rho e_t}{\partial t} + \vec{\nabla} \cdot (\rho \vec{u} h_t) = \rho \vec{g} \cdot \vec{u} - \rho \sum_j \Delta h_{f,j} \dot{\omega}_j + S_{cr} \tag{19}$$

$$\frac{\partial \rho K_0}{\partial t} + \vec{\nabla} \cdot (\rho \vec{u} K_0) = 0 \tag{20}$$

18

$$\frac{\partial \rho Y_{H_2,f}}{\partial t} + \vec{\nabla} \cdot (\rho \vec{u} Y_{H_2,f}) = 0 \tag{21}$$

$$\frac{\partial \rho Y_{H_2,i}}{\partial t} + \vec{\nabla} \cdot (\rho \vec{u} Y_{H_2,i}) = 0 \tag{22}$$

The mass fractions Y_k $(k = H_2, O_2, H_2O)$, the species density ρ_k and the mixture density are related by:

$$Y_k = \frac{\rho_k}{\rho} \tag{23}$$

3.1.1. Combustion modeling

In this section, we describe the reaction rate $\dot{\omega}_k$ present as a source term in Eqs. (17) and (19) and the meaning of the transport Eqs. (20)-(22). This has been presented in details in [23] and we shall briefly present it here for completeness.

In each elementary control volume, we define the combustion progress variable ξ as:

$$\xi(\vec{r}, t) = \frac{Y_{H_2}(\vec{r}, t) - Y_{H_2,i}(\vec{r}, t)}{Y_{H_2,f}(\vec{r}, t) - Y_{H_2,i}(\vec{r}, t)} \tag{24}$$

where Y_{H_2} is the hydrogen mass fraction, and the indices i and f refer to the *unburned* and *burned* mixture (i.e. the mixture before and after combustion), respectively. The reaction rate for the progress variable ξ is :

$$\dot{\omega}_\xi = \frac{K_0}{\Delta x} \cdot \Psi \tag{25}$$

where K_0 (m/s) is a parameter related to the flame velocity, Δx the mesh dimension (we consider here only uniform, or nearly uniform cartesian meshes). Ψ is a criterion function defined as:

$$\Psi = \begin{cases} 1 & \text{if } \varepsilon^2 = \varepsilon^2_{l,m,n} \\ 0 & \text{if not} \end{cases} \tag{26}$$

where

$$\begin{aligned} \varepsilon^2_{l,m,n} = {}& \xi^2_{l+1,m,n} + \xi^2_{l-1,m,n} + \xi^2_{l,m+1,n} + \xi^2_{l,m-1,n} \\ & + \xi^2_{l,m,n+1} + \xi^2_{l,m,n-1} - 3\xi^2_{l,m,n} \end{aligned} \tag{27}$$

and l, m, n are the computational mesh index.

The reaction rates $\dot{\omega}_{H_2}$ and $\dot{\omega}_\xi$ are linked by:

$$\dot{\omega}_{H_2} = (Y_{H_2,f} - Y_{H_2,i})\dot{\omega}_\xi \tag{28}$$

19

and the reaction rates for Y_{O_2}, Y_{H_2O} and Y_{N_2} can be deduced from:

$$\frac{\dot{\omega}_{H_2}}{W_{H_2}} = \frac{\dot{\omega}_{O_2}}{1/2W_{O_2}} = -\frac{\dot{\omega}_{H_2O}}{W_{H_2O}} \tag{29}$$

From Eqs. (25), (28) and (29) we can compute the species reaction rates if we know K_0, $Y_{H_2,f}$ and $Y_{H_2,i}$. These functions depend on the Lagrangian position $\vec{r}_O$, therefore we have to transport these quantities in Lagrangian manner which leads to (20)-(22).

We note that for combustion modeling without spray effect and with initially uniform gas mixture, we do not need to resolve the set of equations (21)-(22), as initial and final hydrogen concentrations are constant both in time and space. When the spray effect is taken into account, these equations, on the contrary, have to be considered as the hydrogen concentration will change due to evaporation process.

The source term S_{cr} which expresses the transfer of energy from the system to its environment, of Eq. (19) is given by:

$$S_{cr} = -H(T - T_0) \tag{30}$$

where H and T_0 are taken constant.

3.1.2. Vaporization modeling study

In this part, we assume an ideal gas mixture and we focus on the thermodynamic aspect of the vaporization of water droplets during the combustion.

In every cell, we consider two successive phenomena: the combustion of the premixed gas mixture, and the vaporization of the liquid phase. In our model, we introduce a criterion to start the vaporization process. When $\xi_i > \xi_{threshold}$, part of a liquid phase evaporates instantaneously in the ith cell with evaporation rate $\dot{\alpha}$ and we find the *updated* variables by conservation laws. We consider the vaporization process inside a closed adiabatic computational cell.

The conservation of mass for the post-evaporation gas phase gives:

$$\widetilde{m}_i^{ini} = \widetilde{m}_i^{fin} = \widetilde{m}_{i,gas}^{ini} + \widetilde{m}_{i,liq}^{ini} \tag{31}$$

The total energy of the system in the ith cell is defined as the sum of two parts: the formation enthalpy and the internal energy and we neglect the kinetic energy. For example, the initial state can be expressed as:

$$\widetilde{e}_i^{ini} = \sum_j Y_{i,j}^{ini} h_j^0 + \int_0^{T_{ini,i}} \left\{ \sum_j Y_{i,j}^{ini} c_{v,j}(T') \right\} dT'$$
$$+ Y_{H2O,i}^{liq} \left(h_{H2O,i}^{liq} - \frac{p_{tot,i}}{\rho_{H2O,i}^{liq}} \right) \tag{32}$$

20

where Y_j are the mass fractions for each specie j, T is the mixture temperature, $c_{v,j}(T)$ and h_j^0 are the constant volume specific heat and the formation enthalpy at 0K of the species j, e is the sensible internal energy.

For the first term of Eq. (32), we use the formation enthalpy at 0 K. Polynomial functions have been used [24] to calculate the heat capacity at constant volume. The internal energy for liquid water is calculated using its specific enthalpy.

Considering the ideal gas hypothesis, the energy at the final state is given by:

$$\widetilde{e}_i^{fin} = \sum_j Y_{i,j}^{fin} h_j^0 + \int_0^{T_{fin,i}} \left\{ \sum_j Y_{i,j}^{fin} c_{v,j}(T') \right\} dT' \\ + Y_{H2O,i}^{liq \to vap} \left(h_{H_2O,i}^{gas} - \frac{RT_{fin,i}}{M_{H_2O}} \right) \tag{33}$$

The conservation of mass and energy in the ith cell gives:

$$\widetilde{e}_i^{ini} = \widetilde{e}_i^{fin} \tag{34}$$

We finally get the governing equations for the vaporization, which will be used to calculate the temperature and the pressure inside the computational cell, assuming ideal gas hypothesis.

3.2. Determination of the parameters in the CREBCOM model

In the CREBCOM model, the thermal conduction and species diffusion are not directly modeled. Their action is taken into account by introducing a correlation derived from experimental data that acts as a source term in Euler equations. The model for the burning rate, parameter K_0, is assumed to be constant throughout the combustion process, resulting in conservative estimations of pressure loads [14]. The parameter H related to heat losses can play an important role for slow flame developments. In this section, we present our strategy for choosing values for the aforementioned parameters.

3.2.1. Determination of the parameter K_0

Determination of visible flame speeds, V_f, is very important for appropriate prediction of pressure loads. To solve this problem, one can imply a model for determination of the appropriate constant K_0, which results in the expected value of visible flame speed [14]. The combustion model in the CREBCOM code uses a value of constant K_0 as an input parameter. A simple analysis of [14] for one-dimensional flame

21

propagation shows that the following correlation between S_T, the so-called turbulent burning rate, and K_0 can be derived:

$$K_0 = \frac{S_T(\sigma + 1)}{4} \tag{35}$$

where $\sigma = \frac{\rho_u}{\rho_b}$ is the expansion ratio, ρ_u and ρ_b are densities of the fresh and burnt gas. This expression may be used to estimate the value of K_0 from correlations for S_T.

For the determination of S_T, and following the estimation of Bradley [25], three correlations are derived according to the flame velocity. For a slow deflagration, the model proposes:

$$\frac{S_T}{S_L} = 0.0008(\sigma - 1)^3 \left(\frac{L_T}{\delta}\right) \quad , \text{for weak turbulence}, \frac{L_T}{\delta} < 500 \tag{36}$$

Table 7: Mixture properties for $x_{H_2} = 16\%$ in database of [26] used in the model of [14]

$x_{H_2}\,[-]$	$\sigma\,[-]$	$S_L\,[m/s]$	Le	$L_T/\delta\,[-]$	$c_{sp}\,[m/s]$
0.16	4.83	0.91	0.4	96	780

For Test 7, by using the parameters chosen in the experiments of [20] (see Table 7), we can calculate the parameter K_0 in the hydrogen-air composition of $x_{H_2} = 16\%$, by referring to Eqs. (35)-(36):

$$K_0 \approx 5.73 \text{ m/s} \tag{37}$$

It should be emphasized that the parameter K_0 is *not* the burning velocity even though it has some similar properties. By implementing transducers in the geometry, we can have the evolutions of visible flame velocity as a function of flame propagation distance in the tube.

Two models [27][28] show that the maximal value for the visible flame velocity cannot reach the sound speed in the combustion product ($c_{sp} = 787$ m/s), in Test 7 ($x_{H_2} = 16\%$). The other set of experiments [26] has given experimental data on flame velocity evolutions with X/D values, for different gas mixtures, blockage ratio etc. It was shown that a maximal flame velocity occurs in the middle of the tube. We can thus deduce that the maximal visible flame velocity cannot exceed a value of 70 m/s in Test 7 of [1].

Using the above arguments in our calculations, we take $K_0 \approx 5.73$ m/s which results in the visible flame velocity varying between 10 m/s and 40 m/s.

3.2.2. Determination of the parameter H

In section 2, it is shown that a) the value of the parameter H can be chosen within the range of $H = 4000\pm50\%$ and b) this parameter *has an important* influence on the maximum pressure value as well as the shape of the pressure signal.

The value of parameter H after completeness of combustion, past t_{max} is different from the value of the parameter during the combustion due to the difference in gas velocity. An additional difficulty lies in the fact that the experimentally obtained pressure signal at later stage is influenced by the temperature, and cannot be reliable [29]. Nevertheless, for Test 7, we have estimated this value, $H_2 = 425 \ W/m^3/K$ by matching numerical and experimental data.

The value $H_1 = 1700 \ W/m^3/K$ chosen for the volumetric heat loss coefficient during combustion is lower than the range prescribed by [20]. Since the tube used in the experiments of [1] is smooth, and the results of [20] were obtained for the blockage ratio, BR > 0. One can argue that the heat loss due to convection is less important in the present case.

In Fig. 12, we present the results for pressure evolution corresponding to Test 7 (no spray) computed with CREBCOM model and the above estimated parameters.
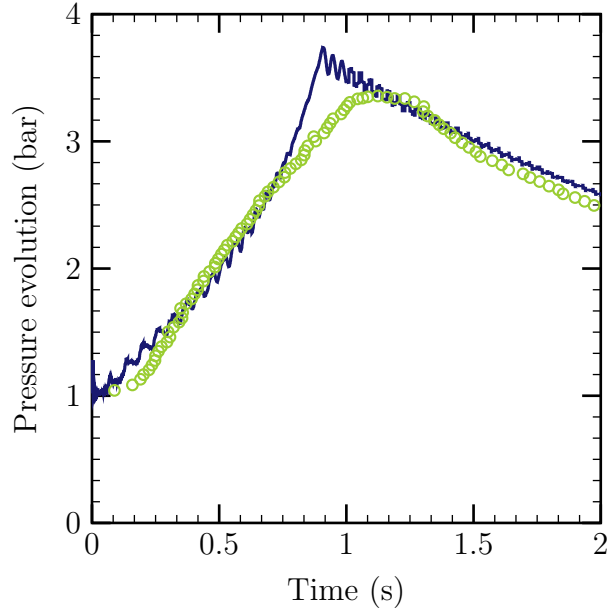

Figure 12: Test 7 (no spray). Pressure evolution as a function of time by setting $H_2 = 1700 \ W/m^3/K$, $H_1 = 425 \ W/m^3/K$. Comparison between experimental ($\circ$) and CFD results (———)

Some important conclusions can be drawn from the Fig. 12. First, we can see that the slopes of the computed pressure evolution are similar to the experimental data, which means that the parameters H are reasonably estimated for this test case. The peak value for pressure p_{max} appears at $t_{max} = 0.9$ s, indicating that the $K_0 = 5.73$ m/s is well estimated. The non-smooth pressure behavior at $t = t_{max}$ can be attributed to abrupt change of parameter H in our calculation.

We mention that we use fully compressible numerical solver, and the acoustic waves are not filtered. The pressure oscillations of the numerical solutions have frequency of $f_{osci}^{num} = 34\ Hz$ which corresponds well to the frequency of acoustic wave travelling back and forth through the burnt gas along the tube, i.e. $f_{acou} = 32\ Hz$.

3.3. Water Spray Effect

After choosing K_0 and H for the combustion, we can focus on the effect of water spray. Test 8 differs from Test 7 by the presence of a water spray of a supply flow rate $Q_w = 4.6$ l/s (see Table 1).

3.3.1. Modeling of Test 8

The transient evolution of the static pressure during the combustion process in the CREBCOM model depends on K_0, H and the evaporation rate of the water droplets. In this section, we present the results for Test 8 with $K_0 = 5.73$ m/s, which is the same as in Test 7, $H_1 = 3850\ W/m^3/K$ and $H_2 = 800\ W/m^3/K$. The values for volumetric heat loss coefficient are higher than those in Test 7. Moreover the value for H_1 lies in range similar to [20]. This is justified by the fact that heat losses due to convection are higher due to the presence of relatively cold droplets.

The flow rate of the water spray system is: $Q_w = 4.6$ l/s, which can be considered to be a theoretical upper limit of the evaporation rate, that is:

$$\dot{\alpha}_{max} = \frac{Q_w}{V_{tube}} \approx 2.9 \times 10^{-3} s^{-1} \tag{38}$$

where V_{tube} is the volume of the main tube i.e. the region with water spray system.

The evaporation process is implemented at every time step, and is characterized by $\dot{\alpha}\ (s^{-1})$. In each computational cell, this equality is related to the evaporated liquid mass during a time step Δt:

$$m_{cell}^{H_2O} = \dot{\alpha}\,\rho_{H_2O}\,V_{cell}\,\Delta t \tag{39}$$

As the value estimated in the reduced-order model (see section 2), we use $\dot{\alpha} = 6.01 \times 10^{-5}\ s^{-1}$ as the mean evaporation rate during the combustion process.
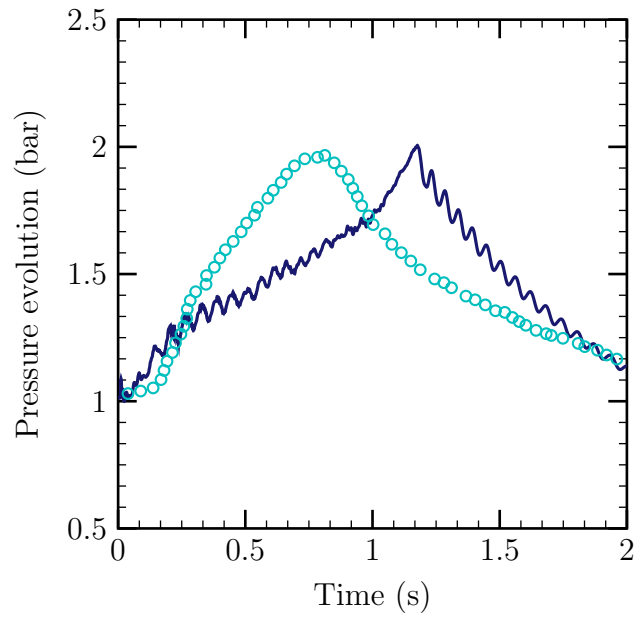
Figure 13: Test 8 (with spray). Pressure evolution for hydrogen-air mixture ($x_{H_2} = 0.16$), with $p_{ini} = 1.013\ bar$, $H_1 = 3850\ W/m^3/K$, $H_2 = 800\ W/m^3/K$, $K_0 = 5.73\ m/s$. Comparison between the experimental results ($\circ$) and CFD calculation results (—)

Fig. 13 shows the calculated pressure evolutio compared to the experimental data of Test 8. It can be seen that by adjusting the parameters K_0, H and $\dot{\alpha}$, it is possible to simulate the mitigation effect of the spray with a reasonable approximation. The maximal value for the pressure p_{max} is close to the experimental one, i.e. $p_{exp}^{max} = 1.9$ bar, $p_{cal}^{max} = 2.0$ bar. It is noticed that the slope of corresponding to the computed evolution differs from experimental counterpart. In fact, as shown in the literature [11] [?], the spray flow from the nozzles can generate turbulence which might lead to the flame acceleration. In Test 7, the peak pressure p_{exp}^{max} takes place at $t_0 \approx 1$ s. However, in Test 8, the time needed to reach the p_{exp}^{max} is equal to 0.7 s, meaning that the flame velocity is higher in the later case. The peak pressure arrives happens at $t \approx 1.2$ s in our simulation.
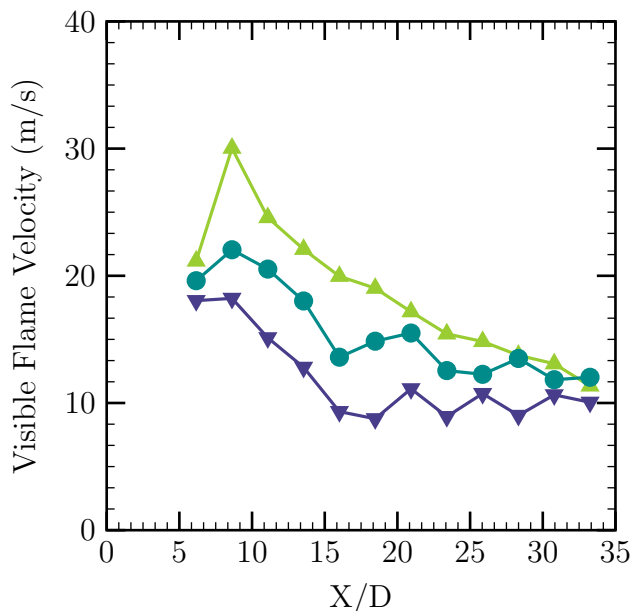

Figure 14: Visible flame velocity evolution for hydrogen-air mixture ($x_{H_2} = 0.16$) AICC combustion, with initial pressure $p_{ini} = 1.013\ bar$ (—▲—); effect of heat losses only (—●—), spray effect (—▼—)

We have computed the visible flame velocity using the flame arrival data from numerical transducers. Fig. 14 shows the evolution of the visible flame speed under the influence of heat loss and the water spray. The calculations are performed by keeping the same value for K_0. We can see that in our model, the heat loss and the spray effect reduce the flame velocity. Compared to the combustion without heat losses, the flame velocity can be decelerated by 5 m/s under the heat loss, and 10

m/s by the spray effect. In order to counterbalance these effects, the value of K_0 should be increased by a factor related to spray-generated turbulence, which however is unknown.

3.3.2. Energy balance analysis

By integrating the energy conservation equation on the computational domain, we can write symbolically:

$$\frac{d}{dt} \int_V \rho \, e_t \, dV = \int_V E_m \, dV + \int_V E_c \, dV + \int_V E_v \, dV$$

where E_m, E_c and E_v denote combustion, convection and evaporation energy losses, respectively.

The first term on the right-hand side is the energy increase rate due to the combustion, while the other two terms are related to the energy loss due to the convective mechanism and the liquid water evaporation. These three terms are respectively characterized by three parameters K_0 (E_m), H (E_c) and $\dot{\alpha}$ (E_v).
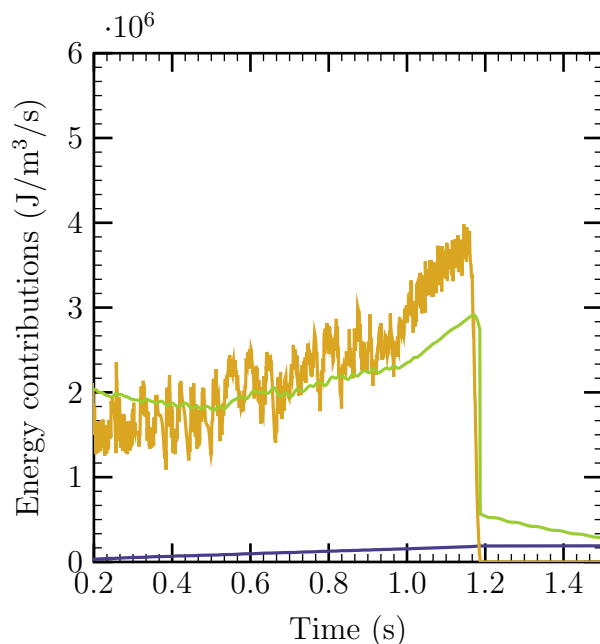

Figure 15: Test 8 (with spray). Evolution of three terms in Eq. (40) : combustion heat (——), convective heat loss (——) and heat losses due to evaporation (——)

Fig. 15 shows the energy change in the tube per unit volume and per second. The combustion process will increase the total energy, while the heat loss and the spray evaporation will consume the energy. From Fig. 15, we can see that the contributions due to the combustion and the convective heat loss are of the same order of magnitude, $\sim 2 - 3 \ MW/m^3$, while the contribution related to heat loss due to droplets evaporation is lower by one order of magnitude, $\sim 0.1 \ MW/m^3$. Again, this confirms the importance of the convection heat losses (see Section 2). The relative increase in the contribution due to combustion, for $1 \ s <$ t $< 2 \ s$ is related to the fact that at the end of the tube, the flame propagates through a pre-compressed mixture having higher energy per unit volume.

3.4. Cell Size Effect

In the CREBCOM model, the size of the numerical cells play an important role. For example, the chemical reaction rate is well related to the mesh cell size Δx. In the former studies, we have investigated the water spay effects by using the geometries having a cell size of $\Delta x = 10$ cm. In this section, we perform mesh sensitivity study, i.e. by considering an averaged mesh size of $\Delta x = 5$ cm.

From Fig. 16, we notice that in our calculation once the mesh size changes from $\Delta x = 10$ cm to $\Delta x = 5$ cm, the parameter K_0 has to be adjusted in order to have similar behavior.

The computed results are given in the Fig. 17, and compared to the experimental data of Tests 7 and 8. Note that by choosing $K_0 = 7.0 \ m/s$, a reasonable approximation between the calculation and the experimental data in Test 7 is found. The slope of the pressure is well estimated. The peak value for the pressure evolution p_{cal}^{max} is slightly higher compared to the experimental data. For Test 8, we have kept the same heat loss coefficient $H_1 = 3850 \ W/m^3/K$ and $\dot{\alpha} = 6.01 \times 10^{-5} \ s^{-1}$ as for the test case with larger mesh size ($\Delta x = 10$ cm). Overall, the change in parameter K_0 is not significant ($< 20\%$) and we can conclude that for the considered tests, dividing by 2 the averaged mesh size, the same model parameters hold.

The higher amplitude of the oscillations corresponding to the numerical solution for pressure at the finer mesh can be attributed to the lower numerical viscosity, i.e. minor damping effect.

4. Conclusion

In this paper, we describe a methodology to determine the pressure loads in a closed volume during turbulent combustion of hydrogen in the presence of water spray.
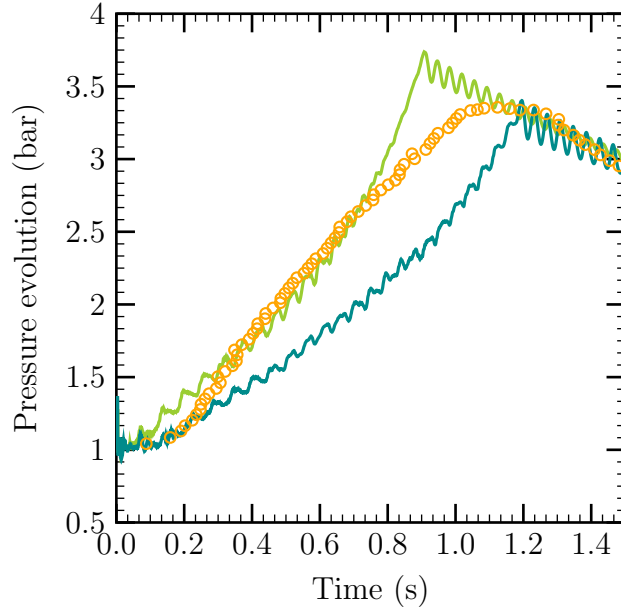
Figure 16: Test 7 (no spray). Pressure evolution for hydrogen-air mixture ($x_{H_2} = 0.16$), with $p_{ini} = 1.013\ bar$, $H_1 = 1700\ W/m^3/K$, $H_2 = 425\ W/m^3/K$, $K_0 = 5.73\ m/s$. The experimental results are given in ($\circ$). Comparison between the coarse mesh $\Delta x = 10\ cm$ (——) and the finer mesh $\Delta x = 5\ cm$ (——)
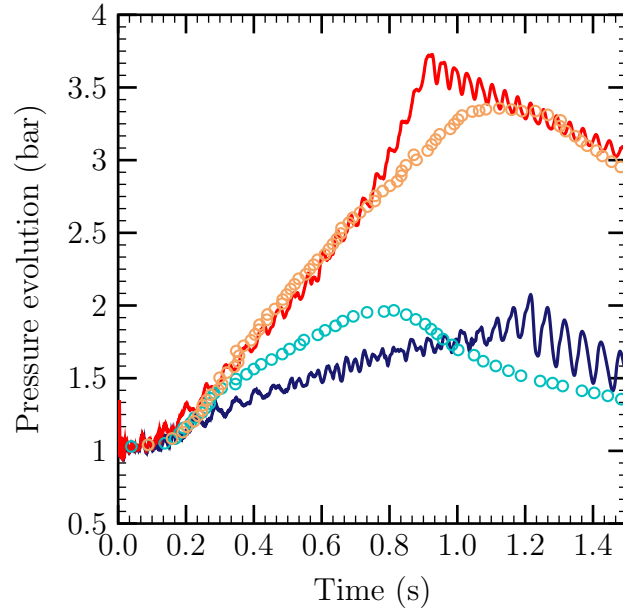
Figure 17: Tests 7 and 8. Pressure evolution for hydrogen-air mixture ($x_{H_2} = 0.16$), with $p_{ini} = 1.013$ bar; for Test 7, $H_1 = 1700$ $W/m^3/K$, $H_2 = 425$ $W/m^3/K$, $K_0 = 7.0$ m/s, for Test 8, $H_1 = 3850$ $W/m^3/K$, $H_2 = 800$ $W/m^3/K$, $K_0 = 7.0$ m/s, $\dot{\alpha} = 6.0 \times 10^{-5}$ s^{-1}, mesh size $\Delta x = 5$ cm. Comparison between the experimental results (no spray ○, with spray ○), and CFD calculation results (no spray ——, with spray ——)

The experimental data are first analyzed using a simplified engineering model. As a result, we could observe that very similar pressure evolutions can be obtained by using different combinations of model parameters. The Design-Of-Experiment method has been employed to perform the sensitivity analysis with respect to the model parameters. It is shown that the volumetric heat loss coefficient due to convection is the most important parameters that influence the maximum pressure and the pressure evolution shape.

Preliminary work has been performed in order to estimate the CFD model parameters such as the flame velocity constant K_0, the heat transfer coefficient H, and the volumetric evaporation rate $\dot{\alpha}$. Due to the lack of accurate data, the choices for these parameters can rely on the theoretical or other experimental results available in the literature.

The CREBCOM combustion model has been modified accordingly and applied in order to determine the transient state of the combustion system, focusing on the evolution of pressure and the flame velocity, with and without water spray, using the previously estimated parameters. The experimental results corresponding to Tests 7 and 8 of [1] are chosen for validation. It is shown that the pressure evolution is strongly affected by the following contributions: *i*) energy increase rate due to combustion, *ii*) convective energy loss rate and *iii*) the energy loss rate due to evaporation. The relative importance of the second contribution has been confirmed.

The calculations colaborate the experimental findings, that the water spray has an effective mitigation effect on the pressure evolution during the turbulent combustion. It shows that the proposed methodology can be applied in order to determine the pressure loads due to combustion in the presence of sprays at large scale. However, there is a room for improvement concerning a more sophisticated estimation of volumetric heat loss coefficient and of liquid evaporation rate, on the one hand, and for flame acceleration factor due to turbulence generated by a spray, on the other hand. This will be the subject of future research works.

Acknowledgement

Appendix A. Simplified numerical model

We present here a simple engineering model for pressure evolution inside a closed volume, developed under Low-Mach number hypothesis.

Let us consider the sensible enthalpy conservation law [17]:

$$\rho\frac{Dh_s}{Dt} = \dot{\omega}_T + \frac{Dp}{Dt} + \nabla \cdot (\lambda \nabla T) - \nabla \cdot \left(\rho \sum_{k=1}^{N} h_{s,k} Y_k \mathbf{V_k} \right) + \tau_{ij}\frac{\partial u_i}{\partial x_j} \tag{A.1}$$

where specific sensible enthalpy h_s, species k diffusion velocity $\mathbf{V_k}$ into the mixture, the viscous tensor τ_{ij}, and the energy release rate due to combustion $\dot{\omega}_T$ are defined as

$$h_s = \int_0^T C_p \, dT', \tag{A.2}$$

$$\mathbf{V_k}\, x_k = -D_k \nabla x_k, \tag{A.3}$$

$$\tau_{ij} = \mu \left(\frac{\partial u_i}{\partial x_j} + \frac{\partial u_j}{\partial x_i} \right) - \frac{2}{3}\mu\frac{\partial u_k}{\partial x_k}\delta_{ij}, \tag{A.4}$$

$$\dot{\omega}_T = -\sum_{k=1}^{N} \triangle h_{f,k}\dot{\omega}_k. \tag{A.5}$$

The Eq. (A.1) can be rewritten as

$$\rho\frac{Dh_s}{Dt} - \frac{Dp}{Dt} = \dot{\omega}_T + \mathcal{D}_{iff}. \tag{A.6}$$

where $\mathcal{D}_{iff}$ represents the diffusion term. For slow flames observed in some of the experiments, like in Tests 7 and 8, where fluid velocity is of the order of 10 m/s, the specific kinetic energy, $\rho|\mathbf{u}|^2/2$, is of the order of 100 $kg/m/s^2$, while the specific internal enthalpy is

$$\rho \int_0^T C_p \, dT' = \rho\overline{C}_p T = \frac{\overline{\gamma}}{\overline{\gamma} - 1}p = \mathcal{O}(10^5 Pa). \tag{A.7}$$

Taking into account the fact that the combustion takes place at low-Mach number regime (the speeds of sound in the fresh and burnt mixture are 376 m/s and 787 m/s, respectively), one can assume that the pressure is only function of time, i.e. the left-hand side of Eq. (A.6) can be written as

$$\frac{d}{dt}\left(\frac{\overline{\gamma}}{\overline{\gamma} - 1}p \right) - \frac{dp}{dt} \approx \dot{\omega}_T + \mathcal{D}_{iff} \tag{A.8}$$

32

We assume that the flame surface separates the gas into fresh and burnt mixture (combustion occurs at flamelet regime), each having constant properties (see Fig. 4).

Integrating the left hand side of Eq. (A.8) over the closed volume V_{tot}, we get

$$\frac{d}{dt}\left[p\left(\frac{\gamma_b}{\gamma_b-1}V_b+\frac{\gamma_f}{\gamma_f-1}V_f-V_{tot}\right)\right],\tag{A.9}$$

where $V_b(t)$ and $V_f(t)$ are the volumes occupied by burnt and fresh gases, respectively. In the above formula we assume pressure equilibrium between burnt and fresh gases (Low Mach number hypothesis).

Integrating over the volume of the energy release rate, we have

$$\int_V \dot{\omega}_T = \Sigma \cdot S_L \cdot \triangle H \cdot \rho_f \cdot Y_{H_2}\tag{A.10}$$

with Σ being the flame surface, S_L the laminar flame velocity, $\triangle h$ the energy release per unit mass of burnt hydrogen gas, ρ_f the fresh gas density, and Y_{H2} the mass fraction of hydrogen gas in the fresh mixture.

The diffusion terms describing the rate of energy losses are often presented in a simplified form as:

$$\mathcal{D}_{iff} = H\,(T-T_0),\tag{A.11}$$

where H is a *volumetric* heat loss coefficient, and T_0 is a reference temperature.

Finally, the ordinary differential equation for the pressure evolution inside the tube can be written as

$$\frac{d}{dt}\left\{p\left(\frac{\gamma_b}{\gamma_b-1}V_b+\frac{\gamma_f}{\gamma_f-1}V_f-V_{tot}\right)\right\} = \Sigma \cdot S_L \cdot \triangle H \cdot \rho_f \cdot Y_{H_2}$$
$$-H\left\{\frac{p}{\rho_b R_b}V_b+\frac{p}{\rho_f R_f}V_f-T_0 V_{tot}\right\}\tag{A.12}$$

In case of spraying, another term has to be included in the right-hand side of Eq. (A.12). This term represents the energy losses related to the water evaporation:

$$-\rho_l \cdot \dot{\alpha} \cdot l \cdot V_b,\tag{A.13}$$

where ρ_l is the liquid density, l the latent heat of evaporation, and $\dot{\alpha}$ the liquid volume fraction rate of evaporation. For simplicity, we assume that the evaporation takes place inside the burnt volume.

Appendix B. Solution algorithm for the simplified model

Given the initial conditions for pressure p_0, temperature T_0, specific heats ratio related to burnt gas γ_b, to fresh gas γ_f, and laminar flame speed S_L. We

- Choose values for

  (a) integral loss coefficient;

  (b) evaporation rate for volume liquid fraction $\dot{\alpha}$;

  (c) ratio of the flame surface to the tube cross-section area N;

  (d) averaged flame velocity v_{flame}^{av} (this value is needed for computing $t_{fin} = L/v_{flame}^{av}$), and a profile for the v_{flame} (here we use parabolic profile, for simplicity)

- Compute L_{flame}, which is the distance travelled by the flame at time t using the flame velocity evolution in time, and deduce the volume of the burnt gas $V_b = L_{flame} \cdot A_{tube}$.

- Calculate the increment of the mass of the burnt gas m_b and the mass of liquid evaporated m_{liq}^{ev} during the time interval Δt.

- Find the density of the burnt ρ_b and the fresh gases ρ_f.

- Compute the right-hand side of the Eq. (1) and deduce the new value of the pressure using classical differential schemes.

Set $S_L = 0$ when the flame reaches the end of the tube.

Appendix C. Evaporation model of a single droplet [19]

Appendix C.1. Gas phase

Here we present here the practical step-by-step procedure of determination of the vaporization rate $\dot{m}$ and the heat transferred into the droplet interior, Q_L. For the justifications the reader can refer to the original article of [19]. Concerning the liquid phase analysis, we assume that the temperature within the droplet is uniform in space although the time is varying.

Assume that we know the droplet surface temperature T_s, velocity U, and the conditions of the free-stream flow: U_∞, T_∞, $Y_{F\infty}$. The solution algorithm is given below.

1. Calculate the molar and mass fluid vapor fractions at the droplet surface

$$x_{Fs} = p_{Fs}/p, \quad Y_{Fs} = x_{Fs}M_F/\sum_i x_i M_i. \tag{C.1}$$

Here, p_{Fs} is the fluid vapor saturated pressure which is evaluated using the appropriate correlations

$$p_{Fs} = p_{Fs}(T_s). \tag{C.2}$$

2. Calculate the average physical properties

$$\overline{\rho}, \ \overline{C}_{pF}, \ \overline{C}_{pg}, \ \overline{\lambda}_g, \ \overline{\mu}_g, \ \overline{D}, \ \overline{Le} = \frac{\overline{\lambda}_g}{\overline{\rho}_g \overline{DC}_{pg}}, \ \overline{Pr}, \ \overline{Sc}$$

in the gas film using the reference conditions given by

$$\overline{T} = T_s + \frac{1}{3}(T_\infty - T_s), \tag{C.3}$$

$$\overline{Y}_F = Y_{Fs} + \frac{1}{3}(Y_{F\infty} - Y_{Fs}). \tag{C.4}$$

3. Calculate the Reynolds number, $Re = 2\rho_\infty |U - U_\infty| r_s/\mu_g$, as well as the Nusselt and the Sherwood numbers for a non-vaporizing droplet:

$$Nu_0 = 1 + (1 + Re \cdot Pr)^{1/3} f(Re) \tag{C.5}$$
$$Sh_0 = 1 + (1 + Re \cdot Sc)^{1/3} f(Re) \tag{C.6}$$

where $f(Re) = 1$ at $Re \leq 1$ and $f(Re) = Re^{0.077}$ at $Re \leq 400$.

4. Calculate the Spalding mass transfer number, B_M, diffusional film correction factor, F_M, modified Sherwood number, Sh^*, and the mass vaporization rate, $\dot{m}$:

$$B_M = \frac{Y_{Fs} - Y_{F\infty}}{1 - Y_{Fs}}, \tag{C.7}$$

$$F_M = (1 + B_M)^{0.7} \frac{ln(1 + B_M)}{B_M}, \tag{C.8}$$

$$Sh^* = 2 + (Sh_0 - 2)/F_M, \tag{C.9}$$

$$\dot{m} = 2\pi\overline{\rho}_g\overline{D}_g r_s Sh^* ln(1 + B_M). \tag{C.10}$$

5. Calculate the correction factor for the thermal film thickness, $F_T = F(B_T)$, using the value of the heat transfer number, B_T^{old}, from either the previous iteration or the previous time step.

6. Calculate the modified Nusselt number, Nu^*, the parameter ϕ and the corrected value of the heat transfer number, B_T:

$$Nu^* = 2 + (Nu_0 - 2)/F_T, \qquad (C.11)$$

$$\phi = \left(\frac{\overline{C}_{pF}}{\overline{C}_{pg}}\right) \left(\frac{Sh^*}{Nu^*}\right) \frac{1}{Le}, \qquad (C.12)$$

$$B_T = (1 + B_M)^\phi - 1. \qquad (C.13)$$

7. Evaluate the heat penetrating into the liquid phase

$$Q_L = \dot{m} \left(\frac{\overline{C}_{pF}(T_\infty - T_s)}{B_T} - l(T_s)\right) \qquad (C.14)$$

Appendix C.2. Liquid phase

The transient liquid heating inside the droplet uses the *effective conductivity model*. Coupling the calculation of these two phases, we try to estimate the evaporation rate.

The non-dimensional energy equation for the *effective conductivity model* is given as [19]:

$$\phi^2 \frac{\partial Z}{\partial \tau} = \beta \, \eta \, \frac{\partial Z}{\partial \eta} + \frac{1}{\eta^2} \frac{\partial}{\partial \eta} \left(\eta^2 \frac{\partial Z}{\partial \eta}\right) \qquad (C.15)$$

where:

r_s is the current radius of the droplet;
$Z = (T - T_0)/T_0$ is the non-dimensional temperature of the droplet;
$\phi = r_s/r_0$ is the non-dimensional radius of the droplet;
$\eta = r/r_s$ is the non-dimensional coordinate;
$\tau = \alpha_L \, t/r_0^2$ is the non-dimensional time;
α_L is the liquid thermal diffusivity;
β is proportional to the regression rate of the droplet surfaces, which can be estimated by:

$$\beta = -\frac{1}{4\pi\alpha_L\rho_L r_s} \left[\dot{m} + \frac{1}{\rho_L C_{p,L}} Q_L\right] \qquad (C.16)$$

The following parameters have been used in the numerical solution[19][30];

$Pe_L = 2U_s r_0/\alpha_L$ is the liquid Peclet number, where U_s is the maximal surface velocity:

$$U_s = \frac{1}{32}(U_\infty - U) \left(\frac{\mu_g}{\mu_L}\right) Re_g C_F(Re_g) \qquad (C.17)$$

$$C_F = \frac{12.69}{Re_g^{2/3}(1 + B_M)} \tag{C.18}$$

$k_{eff} = \chi\, k_L$ is the effective thermal conductivty coefficient, where:

$$\chi = 1.86 + 0.86\ tanh[2.245\ log_{10}(Pe_L/30)] \tag{C.19}$$

References

[1] Carlson LW, Knight RM, Henrie JO. Flame and detonation initiation and propagation in various hydrogen-air mixtures, with and without spray. Atomics International Div., Canoga Park, Calif. 1973;6:73-29.

[2] Foissac A, Malet J, Vetrano MR, Buchlin JM, Mimouni S, Feuillebois F, Simonin O. Droplet size and velocity measurements at the outlet of a hollow cone spray nozzle. Atomization Sprays 2011;21:893-905. https://doi.org/10.1615/AtomizSpr.2012004171.

[3] Thomas GO, Brenton JR. An investigation of factors on relevance during explosion suppression by water sprays. Health and safety executive-offshore technoloty report; 1996

[4] Thomas GO. On the conditions required for explosion mitigation by water sprays. Process Saf. Environ. Prot. 2000;78:339-54. https://doi.org/10.1205/095758200530862.

[5] Zalosh RG, Bajpai SN. Water fog inerting of hydrogen-air mixtures. Proc. 2nd Int Conf on the Impact of Hydrogen on Water Reactor Safety. New Mexico, USA:1982.

[6] Boech LR, Kink A, Oezdin D, Hasslberger J, Sattelmayer T. Influence of water mist on flame acceleration, DDT and detonation in H_2-air mixtures. Int. J. Hydrogen Energy 2015;40:6995-7004. https://doi.org/10.1016/j.ijhydene.2015.03.129.

[7] Ingram JM, Averill AF, Battersby PN, Holborn PG, Nolan PF. Suppression of hydrogen-oxygen-nitrogen explosions by fine water mist: part 1, burning velocity. Int. J. Hydrogen Energy 2012;37:19250-7. https://doi.org/10.1016/j.ijhydene.2012.09.092.

[8]   Holborn PG, Battersby P, Ingram JM, Averill AF, Nolan PF.   Modelling the mitigation of lean hydrogen deflagrations in a vented cylindrical rig with water fog.   Int. J. Hydrogen Energy 2012;37:15406-22. https://doi.org/10.1016/j.ijhydene.2012.07.131.

[9]   Holborn PG, Battersby P, Ingram JM, Averill AF, Nolan PF.   Modelling the effect of water fog on the upper flammability limit of hydrogen-oxygen-nitrogen mixtures.   Int. J. Hydrogen Energy 2013;38:6896-903. https://doi.org/10.1016/j.ijhydene.2013.03.091.

[10] Wingerden KV, Wilkins B, Bakken J, Pedersen G. The influence of water sprays on gas explosions. Part 2: mitigation. J. Loss Prev. Process Ind. 1995;8:61-70. https://doi.org/10.1016/0950-4230(95)00007-N.

[11] Wingerden KV, Wilkins B. The influence of water sprays on gas explosions. Part 1: water-spray-generated turbulence. J. Loss Prev. Process Ind. 1995;8:53-59. https://doi.org/10.1016/0950-4230(95)00002-I.

[12] ISP-49 on Hydrogen Combustion. Nuclear Energy Agency, https://www.oecd-nea.org/nsd/docs/2011/csni-r2011-9.pdf; 2011.

[13] Cheikhravat H. Etude Expérimentale de la combustion de l'hydrogène dans une atmosphère inflammable en présence de gouttes d'eau. PhD thesis, Université d'Orléans; 2009.

[14]   Efimenko AA, Dorofeev SB,   CREBCOM code system for description of gaseous combustion.   J. Loss Prev. Process Ind. 2001;14:575-81. https://doi.org/10.1016/S0950-4230(01)00049-3.

[15]   Kudriakov S, Beccantini A, Dabbene F, Paillere H, Studer E. Evolution of different H_2-Air combustion models for the simulation of large scale confined deflagrations.   J. Energy Inst. 2006;79:200-6. https://doi.org/10.1179/174602206X161392.

[16]   Yang F, Kudriakov S, Studer E, Zou Z, Yu H.   Numerical analysis of hydrogen risk related to severe accident scenario in chinese PWR. In: 24th internaltional conference of nuclear engineering.   USA:2016. https://doi.org/10.1115/ICONE24-60671.

[17] Poinsot T, Veynante D. Theoretical and Numerical Combustion. 3nd ed. R.T. Edwards Inc.; 2005.

[18] Baker WE, Cox PA, Westine PS, Kulesz JJ, Strehow RA. Explosion hazards and evaluation. 1st ed. Oxford, New York: Elsevier; 1983.

[19] Abramzon B, Sirignano WA. Droplet vaporization model for spray combustion calculations. Int. J. Heat Mass Transf. 1989;32:1605-18. https://doi.org/10.1016/0017-9310(89)90043-4.

[20] Kuznetsov M, Matsukov I, Dorofeev S. Heat loss rates from hydrogen-air turbulent flames in tubes. Combust. Sci. TechnolN. 2002;174:75-92. https://doi.org/10.1080/00102200290021443.

[21] Cavazzuti M. Optimization Methods: From Theory to Design Scientific and Technological Aspects in Mechanics. Springer-Verlag Berlin Heidelberg; 2013.

[22] Montgomery DC. Design and Analysis of Experiments. 5th ed. New York: John Wiley & Sons; 2000.

[23] Beccantini A. Implementation of CREBCOM Combustion Model in TONUS Code. Technical Report CEA/DM2S; 2001.

[24] NIST-JANAF THERMOCHEMICAL TABLES. J. Phys. Chem. Ref. Data.

[25] Bradley D, Lau AKC, Lawes M, Smith FT. Flame stretch rate as a determinant of turbulent burning velocity. Phil. Trans. R. Soc. Lond 1992;338:359-87. https://doi.org/10.1098/rsta.1992.0012.

[26] Kuznetsov M et al. Effect of obstacle geometry on behavior of turbulent flames. Institut fur Kern-und Engergietechnik; 1999.

[27] Dorofeev SB, Kuznetsov M. Hydrogen flames in tubes: critical run-up distances. Int. J. Hydrogen Energy 2009;34:5832-37. https://doi.org/10.1016/j.ijhydene.2009.01.008.

[28] Silvestrini M, Genova B, Parisi G, Leon FJ. Flame acceleration and DDT run-up distance for smooth and obstacles filled tubes. J. Loss Prevent. Proc. 2008;21:555-62. https://doi.org/10.1016/j.jlp.2008.05.002.

[29] Chaumeix N. Private Communications.

[30] Abramzon B, Sazhin S. Droplet vaporization model in the presence of thermal radiation. Int. J. Heat Mass Transf. 2005;48:1868-73. https://doi.org/10.1016/j.ijheatmasstransfer.2004.11.017.